Optimal retrieval method to estimate ozone vertical profile in the mesosphere and lower thermosphere (MLT) region from submillimeter-wave limb emission spectra

K. Kuribayashi[a,b], N. Yoshida[a], H. Jin[b], Y. J. Orsolini[c], Y. Kasai[b,a,*]

[a] *Tokyo Institute of Technology, 4259 Nagatsuta-cho, Midori-ku, Yokohama, Kanagawa 226-8503, Japan*
[b] *National Institute of Information and Communications Technology, 4-2-1 Nukui-kitamachi, Koganei, Tokyo 184-8795, Japan*
[c] *Norwegian Institute for Air Research, Instituttveien 18, 2007 Kjeller, Norway*

Abstract

Spectrum width and intensity of ozone (O_3) observed in the MLT region behaves quite differently than in the stratosphere for submillimeter-wave limb emission spectroscopic observation. For example, O_3 spectra in the stratosphere are stronger during the day than at night. Conversely, spectra in the MLT region at night are stronger than those occurring during the day due to diurnal variations in O_3 behavior. These opposing behaviors cause problems, including oscillations and inaccuracies particularly for O_3 vertical profiles in the MLT region retrieved with an application of one retrieval procedure for the entire vertical range (stratosphere to thermosphere). Recently, we developed an optimal retrieval method for O_3 in the MLT region for spectra, observed by the Superconducting Submillimeter-Wave Limb-Emission Sounder (SMILES) instrument on the International Space Station. Optimizations were performed for frequency window range, retrieval vertical range, vertical grids, and a priori information for O_3 and temperature. Precision and accuracy were evaluated by error analysis and comparisons with previous products. The random error was estimated to be about 5% and 35% in the mesosphere and lower thermosphere, respec-

*Corresponding author
Email address: ykasai@nict.go.jp (Y. Kasai)

tively, for nighttime O_3 profiles in the MLT region. The total systematic error was about 6% in the MLT region. Certain improvements for both random noise (from 50% to 35%) and systematic error (from 10% to 6%) were obtained. We succeeded in revealing the positive correlation between O_3 and ClO at nighttime in the upper mesosphere using the optimized O_3 profiles; furthermore, its chemical mechanism was explained quantitatively.

Keywords: SMILES, Ozone, MLT region

1. Introduction

Ozone (O_3) plays important roles as a major absorber of UV-VIS radiation in the Earth's middle atmosphere and as a thermal infrared cooler in the mesosphere [1, 2]. Observations of mesospheric O_3 have been reported since the 1970s [3], and there are many studies of mesospheric O_3 using satellite measurements over the past decade [4, 5, 6]. The O_3 in the mesosphere and lower thermosphere (MLT) region shows a diurnal variation: an enhancement at the beginning of night but a decrease during the day [7, 8]. This behavior in the MLT region is opposite to that which occurs in the stratosphere. A quantitative understanding of the chemical, dynamical, and radiative behavior of O_3 is still needed to improve the understanding of the atmospheric system in the MLT region.

The former O_3 profiles retrieved from submillimeter-wave limb emission spectra have large errors and oscillations in the MLT region, compared with those in the stratosphere. For example, O_3 profiles retrieved from the spectra by the Earth observing system microwave limb sounder on the aura Satellite (Aura/MLS) have a precision of 0.15% and 150% at the pressure height of 5 and 0.05 hPa, respectively [9]. There are two main reasons for this; firstly, the conditions of the retrieval procedures were optimized for the stratospheric O_3. Secondly, all of the former O_3 profiles were obtained by the application of a one-retrieval procedure, with the same conditions from the stratosphere to the lower thermosphere. There had been no O_3 retrieval procedures optimized for

the MLT region.

In this study, we optimized an O_3 retrieval method for O_3 profiles in the MLT region using spectra observed by the Superconducting Submillmeter-Wave Limb-Emission Sounder (SMILES) instrument on the Japanese Experiment Module (JEM) of the International Space Station (ISS) by improving of the frequency window range, the retrieval vertical range, the vertical grids, and the a priori profiles of O_3 and temperature. Error analysis and comparison with past retrieval results were performed to evaluate the precision and accuracy. Furthermore, we showed the positive correlation between chlorine monoxide (ClO) and O_3 in the polar region, and quantitatively explained the chemical mechanism using accurate measurements of O_3 in the MLT region for the first time.

A description of the MLT optimal retrieval method is given in Sect. 2, including the SMILES O_3 observation characteristics (Sect. 2.1). MLT O_3 profiles are evaluated in Sect. 3 with an error analysis (Sect. 3.1), an internal comparison (Sect. 3.2), and a comparison with previous products (Sect. 3.3). Section 4 demonstrates the scientific application using evaluated O_3 profiles in the MLT region. A summary of the work is presented in Sect. 5.

2. Optimization of retrieval method for the O_3 profiles in the MLT region

Section 2.1 describes the observation of O_3 in the MLT region, including the unique nature of the SMILES instrument from the ISS. The optimal retrieval method, with an MLT condition of vertical range, vertical grids, and frequency window is provided in Sects. 2.2 and 2.3. The a priori profiles and their covariance setups, such as O_3, temperature, and pressure, are described in Sect. 2.4.

2.1. SMILES O_3 *spectrum observation and retrieval procedure in general*

We performed O_3 measurements over a wide vertical region, covering the upper troposphere to the lower thermosphere. Measurements were taken using

the SMILES instrument from the ISS between October 12, 2009, and April 21, 2010. The ISS has a non-sun-synchronous circular orbit that allows us to obtain the diurnal variations of observed atmospheric compositions with zonal mean averages. The inclination angle of orbit is 51.6^o to the equator. The nominal latitudinal coverage was 38^o S to 65^o N, since SMILES antenna tilted 45^o from the forward direction. The coverage between 65^o S and 38^o N occurred three times in total, for about 3 weeks during the observation period when the ISS performed a yaw maneuver by 180^o. The number of global measurements was about 1630 vertical limb scans per day. The JEM/SMILES mission is a joint project of the National Institute of Information and Communications Technology (NICT) and the Japan Aerospace Exploration Agency (JAXA).

The SMILES instrument employs a 4 K superconductive heterodyne receivers and the system noise temperature is about 330 K (single-side-band condition). This is about 10–40 times lower than similar space instruments: for example, 3000 K (single-side-band condition) for the Sub-millimetre and Millimetre Radiometer (SMR) on The Odin satellite [10], and 12,000 K (double-side-band condition) for Aura/MLS [11]. This low system noise temperature provides spectra with a 3–6 times better signal-to-noise ratio (SNR) than these other instruments. SMILES O_3 measurements have been investigated in previous research [12, 13, 14, 15, 16], and the details of the SMILES O_3 measurement have been given by Kasai et al. [17].

The SMILES O_3 observation in the MLT region includes the center frequency of the O_3 spectrum at 625.371 GHz, which quantum numbers of rotational transition denoted $(J, K_a, K_c) = (15, 6, 10) - (15, 5, 11)$ [18]. The 625.371 GHz O_3 was measured in two SMILES observation frequency bands, Band-A (624.32–625.52 GHz) and Band-B (625.12–626.32 GHz). The SMILES instrument employs two Acousto-Optical Spectrometer (AOS) with a bandwidth of 1.2 GHz and a frequency resolution of about 1.4 MHz, which are denoted as AOS1 and AOS2 in this study. There are three instrumental configurations for the measurement of the 625.371 GHz O_3 transition; (1) Band-A with AOS1, (2) Band-A with AOS2, and (3) Band-B with AOS2. Kasai et al. [17] provide

more detailed explanations of the instrumental configuration and observation sampling patterns of the SMILES measurements.

The SMILES operational products were developed by both NICT and JAXA. The details of the operational retrieval algorithms of NICT and JAXA were given by Baron et al. [19] and Takahashi et al. [20], respectively. The latest products included NICT-SMILES Level-2 product version 2.1.5 (v215), version 3.0.0 (v300), and JAXA-SMILES Level-2 product version 2.4 (v2.4). We used the SMILES L1b version 008 calibrated spectra [21].

The algorithm for the retrieval used is based on the NICT-SMILES level 2 retrieval algorithm version 2.1.5. In each retrieval process, a solution of the retrieval state vector $\boldsymbol{x}$ of n_x elements is determined by the maximum a posteriori (MAP) method of the non-linear Gaussian case. It is equal to minimizing the following cost function χ^2:

$$\chi^2 = \frac{(\boldsymbol{y} - \mathcal{F}(\boldsymbol{x}, \boldsymbol{b}))^{\mathrm{T}} \mathbf{S}_y^{-1} (\boldsymbol{y} - \mathcal{F}(\boldsymbol{x}, \boldsymbol{b})) + (\boldsymbol{x}_a - \boldsymbol{x})^{\mathrm{T}} \mathbf{S}_a^{-1} (\boldsymbol{x}_a - \boldsymbol{x})}{n_y + n_x}, \tag{1}$$

where $\boldsymbol{y}$ is the measurement vector of n_y elements. $\mathcal{F}(\boldsymbol{x}, \boldsymbol{b})$ is the forward model depending on $\boldsymbol{x}$ and the known model parameter $\boldsymbol{b}$. $\mathbf{S}_y$ is the covariance matrix of the measurement noise and used as a diagonal matrix with elements $(0.5\mathrm{K})^2$ for the retrieval. Lastly, $\boldsymbol{x}_a$ is the a priori value of $\boldsymbol{x}$, and $\mathbf{S}_a$ is the a priori covariance matrix.

The solution that minimizes χ^2 was determined by a Gauss-Newton iterative procedure:

$$\boldsymbol{x}_{r+1} = \boldsymbol{x}_r + (\mathbf{K}_r^{\mathrm{T}} \mathbf{S}_y^{-1} \mathbf{K}_r + \mathbf{S}_a^{-1} + \gamma \mathbf{D})^{-1} \left[\mathbf{K}_r^{\mathrm{T}} \mathbf{S}_y^{-1} (\boldsymbol{y} - \mathcal{F}(\boldsymbol{x}_r)) - \mathbf{S}_a^{-1} (\boldsymbol{x}_a - \boldsymbol{x}_r) \right], \tag{2}$$

where r indicates the number of iterations, $\mathbf{K}_r$ is the weighting function at r^{th} state $\boldsymbol{x}_r$, γ is the Levenberg-Marquardt parameter, and $\mathbf{D}$ is the diagonal matrix with the diagonal elements of $\mathbf{S}_a$. A detailed description for the NICT-SMILES v215 product and its performance can be found in Baron et al. [19] and Kasai et al. [17].

2.2. Optimization of retrieval vertical range and grid for the MLT region

In all of the previous SMILES products, the retrieval procedure to obtain vertical profiles of O_3 was applied from the upper troposphere to the lower thermosphere. With the large differences between the stratosphere (15–50 km) and mesosphere (50–80 km), and given the intensity and width of the O_3 spectrum, we found that an application of one retrieval procedure for the entire vertical altitude was not appropriate for O_3 in the MLT region. The full width at half maximum (FWHM) of the O_3 spectrum at the frequency of 625.371GHz during the night is about 120 and 2 MHz at about 30 and 60 km, respectively. Also, O_3 in the stratosphere is abundant during the day and depleted at night, but the opposite is true in the MLT region [5]. This is one of the reasons for the oscillation of the O_3 profiles in the MLT region.

The usage range of the spectra was optimized for O_3 in the MLT region to a tangent height range between 45 and 110 km. Figure 1 shows an example of the O_3 spectra in the MLT region from a single scan measurement observed by SMILES in the daytime (left panel) and in the nighttime (right panel). The horizontal axis is the frequency grid which is offset to the 625.371 GHz O_3 transition, and the vertical axis is the Brightness Temperature (BT). As shown in Fig. 1, there is a difference in the BT value at 0 MHz, between daytime and nighttime, due to the diurnal variation of O_3. The SNR of the SMILES spectrum was calculated from the value of the BT value at 0 MHz for use as the signal, and the median value of the BT above 10 MHz and under -10 MHz was used as the noise. The typical SNR of the SMILES spectrum in the daytime is smaller than 1.0 above a tangent height of 80.0 km. Hereafter we name this product "SMILES v310".

Optimization of the forward and inversion calculations for the MLT region are: 1) vertical range of O_3 is 50-110 km; 2) vertical grids were 4-km and 2-km for 50–84 km and 84–100 km, respectively. The grid spacing of 2-km in the altitude range 84-100 km was optimized to the secondary ozone maximum around 95 km.

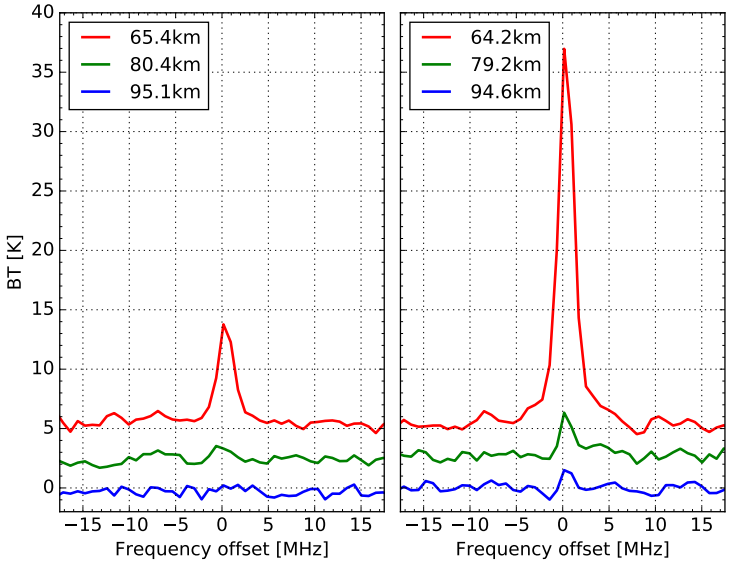

Figure 1: An example of the ozone spectrum observed by SMILES from a single scan measurement in the daytime (left) and nighttime (right). Tangent heights are about 65, 80, and 95 km. An offset of 2.5 and 5.0 K is added for the two lower tangent height spectra, respectively. The frequency axis is shown as an offset from the frequency of the 625.371 GHz O_3 transition.

2.3. Optimization of retrieval frequency window configurations for MLT O_3

We set the frequency windows between 625.3 and 625.45 GHz (120 MHz) and retrieved only ozone in the MLT region, since the line width of the 625.371 GHz ozone spectrum becomes narrower than the SMILES spectral resolution (1.4 MHz) above the upper mesosphere (∼75 km). A lack of contamination species was confirmed in the O_3 window. The former NICT-SMILES O_3 retrieval calculation used spectrum windows with 625.042 and 625.612GHz (570MHz) in both Band-A and Band-B, and retrieved several other parameters, including atmospheric continuum, humidity, hypochlorous acid, ozone isotopomers, and temperature, simultaneously. Moreover, the JAXA-SMILES O_3 retrieval calculation used a spectrum window with all of observed frequency ranges for each Band-A and Band-B and simultaneously retrieved more parameters than any of the former NICT-SMILES products.

These vertical and frequency optimizations allow for the calculation speed

to be increased by more than a factor of 15.

2.4. Improvement of a priori information for diurnal variation of O_3

We improved the usage of a priori profiles by using three-dimensional model calculations in the MLT region.

2.4.1. O_3 *vertical profiles*

The former v215 retrieval calculation used the unique profile from the Goddard Earth Observing System Model version 5.2 (GEOS-5.2) [22] for the mesosphere. This profile was extrapolated to the lower thermosphere. There was no diurnal variation, zonal change, or secondary ozone maximum. The v300 and v2.4 retrieval calculations used a monthly average for 2005–2007 from the Aura/MLS v2.2 [11, 23] data with diurnal and zonal trends.

Here, we used a priori profiles of O_3 from the Whole Atmosphere Community Climate Model version 4 (WACCM4) driven with specified dynamical fields (SD-WACCM) calculations [24, 25]. The specified dynamical fields mean that the meteorological fields in the troposphere and stratosphere are constrained to the Global Modeling and Assimilation Office Modern-Era Retrospective Analysis for Research and Applications [26]. The reasons why we used the SD-WACCM calculations were that it has a vertical grid from surface to 150 km and these calculations well validated the data in the MLT region obtained by comparing Sounding of the Atmosphere using Broadband Emission Radiometry instruments on the Thermosphere Ionosphere Mesosphere Energetic Dynamics satellite (TIMED/SABER) [6]. It was reported that the SD-WACCM O_3 Volume Mixing Ratio (VMR) at the secondary ozone maximum in the nighttime was about 2 times smaller than the O_3 VMR observed by TIMED/SABER, although the day/night differences were well simulated.

The latitudinal variations in the O_3 VMR for both daytime and nighttime were calculated using the SD-WACCM results during the SMILES observation period. The numbers of the SD-WACCM O_3 profiles were averaged for each 10^o latitudinal bin. Nighttime and daytime is defined as occurring when the solar

zenith angle (SZA) is smaller than 75.0° and larger than 105.0°, respectively. These latitudinal variations were interpolated linearly for each SMILES observation point and time from the nearest zonal position and SZA to provide the applicable profile.

The a priori covariance matrix $\mathbf{S}_a$ in Eq. 1 was calculated from the following equation:

$$\mathbf{S}_a[i,j] = \boldsymbol{\epsilon}_a[i]\boldsymbol{\epsilon}_a[j]\exp\left[-\frac{|\boldsymbol{h}[i]-\boldsymbol{h}[j]|}{h_c}\right], \tag{3}$$

where i and j in square brackets indicate the index of a matrix of a vector. $\boldsymbol{h}$ is the vector of the altitude, and the correlation length h_c was set to be 3km. $\boldsymbol{\epsilon}_a$ is a variation in the a priori profiles and was calculated as follows:

$$\boldsymbol{\epsilon}_a[i] = 0.5 \times \boldsymbol{x}_a + 3.0 \times 10^{-7}. \tag{4}$$

We used $\mathbf{S}_a$ as tuning parameters to obtain a stable retrieval.

2.4.2. Temperature and pressure profiles in the MLT region

All previous SMILES O_3 products used the climatology datasets and extrapolated from the stratospheric GEOS-5.2 reanalysis meteorological datasets. The climatology datasets used in the MLT region were Mass Spectrometer and Incoherent Scatter (MSIS) [27] for the SMILES O_3 products v215, and Aura/MLS climatology for v300 and v2.4. A non-smoothing profile and far-from-the-right temperature and pressure provided the oscillated O_3 profile in the MLT region.

We continuously smoothed the temporal and spatial change profile of temperature by using a modeling profile for the global atmosphere in its entirety, from the ground to the ionosphere, called the Ground-to-topside model of Atmosphere and Ionosphere for Aeronomy (GAIA). By using GAIA temperature values, we could conserve the internal consistency between altitude and temperature. The details of the GAIA model are described in Jin et al. [28]. The pressure profile in the MLT region used the hydrostatic equilibrium using the GAIA model data and the reference altitude set to 40 km.

A summary of the optimization of the v310 O_3 product compared with previous products is shown in Table 1.

Table 1: Summary of the retrieval configuration of the NICT-SMILES products and the JAXA-SMILES product.

Versions	v310	v215	v300	v2.4
L1b version	008	007	008	008
Altitude range [km]	45–110	16.5–100	16.5–100	7.5–120
Altitude step [km]				
-Mesosphere	4.0	4.0	4.0	2.5
-Lower thermosphere	2.0	6.0	6.0	2.5
Frequency range [GHz]	625.3–625.45	625.042–625.612	625.042–625.612	624.26-625.59
				625.06-626.38
Target Species	O_3	O_3, ^{18}OOO, $O^{17}OO$, HNO_3, CH_3CN,		
		HOCl, $H^{37}Cl$, $H^{37}Cl$, BrO, HO_2, Temperature		
Temperature	GAIA	GEOS-5.2 + MSIS	GEOS-5.2 + MLS	GEOS-5.2 + MLS
a priori of O_3	SD-WACCM	GEOS-5.2	MLS	MLS

2.5. O_3 *profile in the MLT region from the v310 products*

Figure 2 shows an example of the O_3 profile in the MLT region from the v310 products. The left panel shows the retrieved O_3 profile from the single scan measurement with information on the 1σ retrieval error and vertical resolution. The retrieval error is the root sum of squares of the measurement noise and smoothing errors. The vertical resolution is estimated from the half-width full maximum of the averaging kernel profile ($\mathbf{A}$):

$$\mathbf{A} = (\mathbf{K}^{\mathrm{T}}\mathbf{S}_y^{-1}\mathbf{K} + \mathbf{S}_a^{-1})^{-1}\mathbf{K}^{\mathrm{T}}\mathbf{S}_y^{-1}\mathbf{K}, \tag{5}$$

where $\mathbf{K}$ is the weighting function at the final iteration step. $\mathbf{A}$ describes the sensitivity of the retrieved O_3 profile to the true state. The vertical resolution of the v310 products for single-scan measurements is about 4 km, 10 km, and 7 km in the mesosphere, mesopause, and the lower thermosphere, respectively.

The right panel shows $\mathbf{A}$ and the measurement response ($\boldsymbol{m}$) from a single

scan measurement. $\boldsymbol{m}$ is calculated from $\mathbf{A}$ as follows:

$$\boldsymbol{m}[i] = \sum_j |\mathbf{A}[i,j]|. \tag{6}$$

The unique values of $\boldsymbol{m}$ indicate contributions coming from the retrieved state and a no a priori state.

We assessed the quality of the retrievals using the goodness of the fit based on χ^2 in Eq. 1 and $\boldsymbol{m}$ in Eq. 6; χ^2 smaller than 1.2 is the data selection threshold for removing poorly-fitted scans; $\boldsymbol{m}[i]$ is larger than 0.8 and smaller than 1.2 for each altitude. The flag of the field of view conditions is smaller than 32. This flag indicates there were obstructions to the SMILES field of view by the ISS solar paddles. These criteria provided a useful range of the v310 ozone products from a single scan measurement as 50-101 km and 50–92 km for the nighttime ozone and daytime ozone, respectively.

The measurement response used here has a strong correlation with this maximum tangent height. Since the vertical range of scanning of the SMILES limb observation was random [17], the mean value and standard deviation of the maximum tangent height was given as 97±4 km (1σ).

3. Evaluation of O_3 profiles in the MLT region

We evaluated O_3 profiles in the MLT region (v310 products) by an error analysis, an internal comparison, and a comparison with previous SMILES products.

3.1. Error analysis

Error sources for the O_3 retrieved vertical profiles can be separated into systematic and random errors. Systematic errors come from parameterization of instrumental function, radiative transfer calculations, and also physical parameters that constrain the retrieval procedure. Random errors come from the measurement noise and a priori covariance. The SMILES O_3 spectrum has a SNR of more than 100 in the stratosphere and systematic errors are the major error source [17]. SMILES O_3 spectrum in the MLT region has a small SNR (about 4 around 80 km in the nighttime) as shown in Fig. 1.

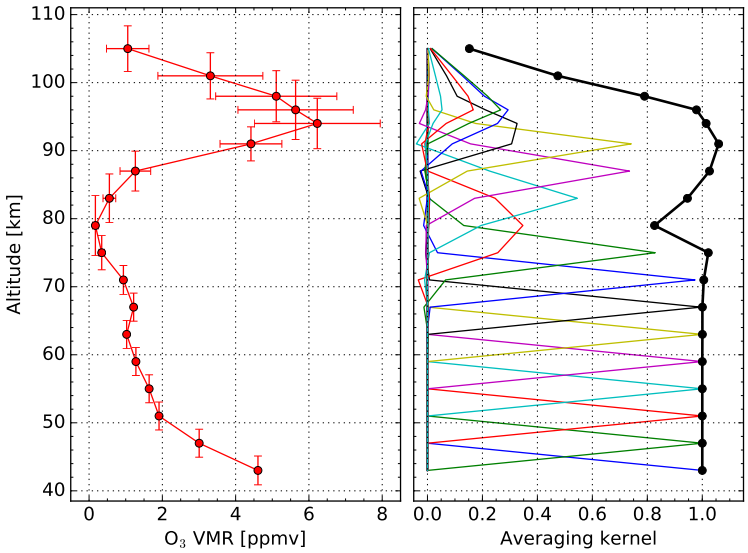

Figure 2: An example of the ozone retrieval from a single-scan measurement in the nighttime. The left panel shows the retrieved ozone profile with vertical and horizontal bars indicating the vertical resolution and the measurement error, respectively. The right panel shows the averaging kernels of the retrieval (colored lines) and the measurement response (thick black line).

Systematic error of SMILES stratospheric O_3 was estimated by perturbation error analysis with one to two major parameters [29, 17, 30] since random error was not a major error source for the good SNR. We evaluated the systematic error value by developing the statistically significant perturbation method for SMILES O_3 in the MLT region spectra to see the effect of the sum of the spectrum noise (averaged the random error).

In the statistically significant perturbation method, the perturbed profiles are calculated from the inversion process with the assumed perturbation parameter using N number of observed spectra as follows:

$$\boldsymbol{x}_p^k = \mathcal{I}(\boldsymbol{y}_{obs}^k, \boldsymbol{b} + \boldsymbol{\Delta b}). \tag{7}$$

Where $\boldsymbol{x}_p^k$ is the perturbed profiles at k^{th} of the N number of observed spectra used, $\mathcal{I}$ is the inversion function, and $\boldsymbol{\Delta b}$ is the perturbed model parameter.

The spectra used in the statistically significant perturbation method were extracted in the equatorial region (5° S – 5° N) in all SMILES observation periods. These spectra numbered about 4,000 and 3,000 for the nighttime and daytime, respectively. We considered that these numbers were enough for the statistically significant condition to reduce the effect of random errors.

The relative difference δ_{rel} between $\boldsymbol{x}_p$ and the v310 standard profiles $\boldsymbol{x}_s$ was calculated as follows:

$$\delta_{rel} = \frac{\boldsymbol{x}_p - \boldsymbol{x}_s}{(\boldsymbol{x}_p + \boldsymbol{x}_d)/2}, \tag{8}$$

where $\boldsymbol{x}_p$ and $\boldsymbol{x}_s$ satisfy the quality of the retrievals defined at the beginning of Sect. 3. The systematic errors were estimated from the median and the median absolute difference (MAD) of δ_{rel} values.

The conditions of the error analysis for the systematic errors were selected on the basis of the previous analysis and summarized in Table 2. It should be noted that Sect. 2.4 describes a large relative difference of about 30% between the SD-WACCM calculations and the TIMED/SABER measurements at the secondary ozone maximum. We used the value of 50% as the perturbation parameter to evaluate the effect on a priori usage.

Figures 3 and 4 show the systematic errors estimated for the v310 O_3 products in the nighttime and in the daytime, respectively. These figures also plot the median values of the smoothing error and measurement noise error for a single scan observation. The total systematic error, labeled as "Total" in Figs. 3 and 4, was calculated as the root sum of squares of all error factors. We performed the same analysis for Band-B and other latitudinal ranges, and the results showed agreements within the MAD values of systematic errors.

The total systematic errors in the nighttime were about 6% in the MLT region, excluding the mesopause ($\sim$ 80.0 km). The total systematic error around the mesopause was about 10%. We used an uncertainty value of 50% for the a priori profiles above 85 km, and the a priori systematic errors in the nighttime were evaluated to be about 6% in this altitude region. The total systematic errors were about 6% for daytime conditions in the lower and middle mesospheres.

Table 2: Systematic errors and their perturbations considered in this study.

Error source	Perturbation
Spectroscopic parameters of O_3	
Air pressure broadening, γ	3%
Temperature dependence, n	10%
Instrumental functions	
AOS response function width	5%
A priori of O_3	
below 85 km	15%
above 85 km	50%

The total systematic error was about 8% and 12% in the upper mesosphere and lower thermosphere, respectively.

The smoothing error and the measurement noise error were relatively larger than the systematic errors for a single scan in the region of the upper mesosphere and the lower thermosphere. In the altitude region where the smoothing error is larger than 40%, the total systematic errors become larger than other altitude region in both of the daytime and nighttime. This means that profile averaging does not provide a sufficient effect to reduce the smoothing error in the case of small amounts of O_3, related to small SNRs in the O_3 spectrum.

3.2. Internal comparison for two different spectra obtained by the same observation condition

SMILES observed the ozone 625.371 GHz transition by two differential frequency ranges, as we described in Sect. 2.1. We compared two ozone profiles retrieved from Band-A and Band-B, both of which observed the same atmospheric air mass.

Figure 5 shows the comparison of the O_3 profiles between Band-A and Band-B using the measurements of the Band-A + Band-B configuration with the median absolute difference. The data are from the latitudinal range of 30^o S – 30^o N in December 2009, for day and night conditions, in order to obtain

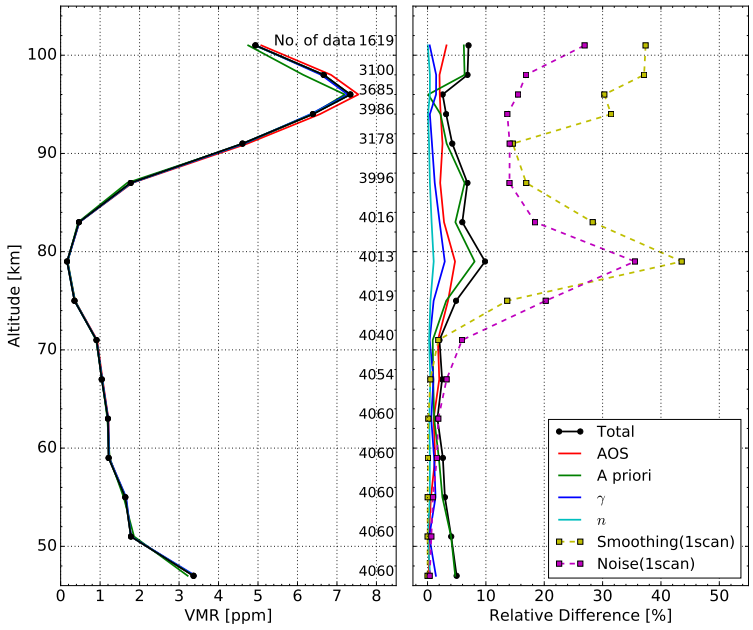

Figure 3: Systematic errors estimated for O_3 in the MLT region (v310 product) in the equatorial region (5° S – 5° N), using all SMILES observation periods from Band-A in the nighttime. The left panel shows the median O_3 profiles retrieved with each error source. The number of data points with good quality criteria is plotted in the left panel. The right panel shows the relative errors for the systematic errors with the median values of the smoothing error and measurement noise error for a single scan. The error sources and the estimated uncertainties are listed in Table 2.

continuous SMILES spectrum under the continuous measurements of the Band-A + Band-B configuration. The median and the median absolute difference of the absolute and relative differences are also plotted in Fig. 5. Note the relative difference is defined as the ratio to the reference ozone profile, which is the mean of the two compared profiles.

The relative differences between Band-A and Band-B in the MLT region are within about 3%, indicating that the different values are smaller than the estimated systematic errors shown in Figs. 3 and 4. We consider that these relative differences between Band-A and Band-B are caused by spectrum noise. We performed the same analysis for other latitudinal and time ranges, and

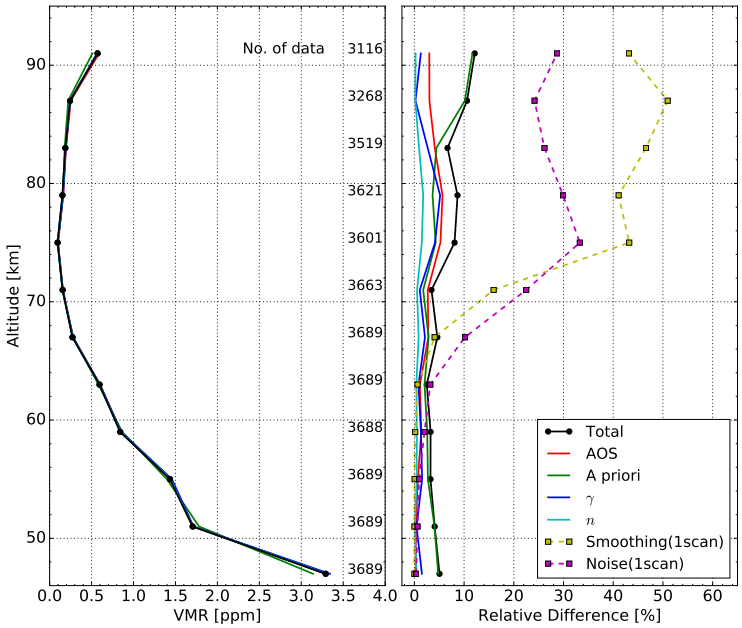

Figure 4: Daytime values for Fig. 3.

there were the agreements within the MAD values of the relative differences. Hereafter, we use O_3 profiles from both Band-A and Band-B.

3.3. Comparison with previous SMILES products

We performed a comparison of the v310 O_3 profiles with those retrieved by the previous NICT and JAXA products. The NICT products used both v215 and v300 since we did not report the error of the v300, and the JAXA products are from v2.4 which is the final version from JAXA. The differences in retrieval conditions are summarized in Table 1. The differences in the processing between v215 and v2.4 are described in Kasai et al. [17] and Imai et al. [13], and the O_3 profiles retrieved by v2.4 processing are compared with other measurements in Smith et al. [15].

The quality selection criteria for v215 and v300 products are a measurement response larger than 0.8 and smaller than 1.2, the goodness of fit is smaller than 1.2, and the flag of the field of view conditions is smaller than 32 [12]. The

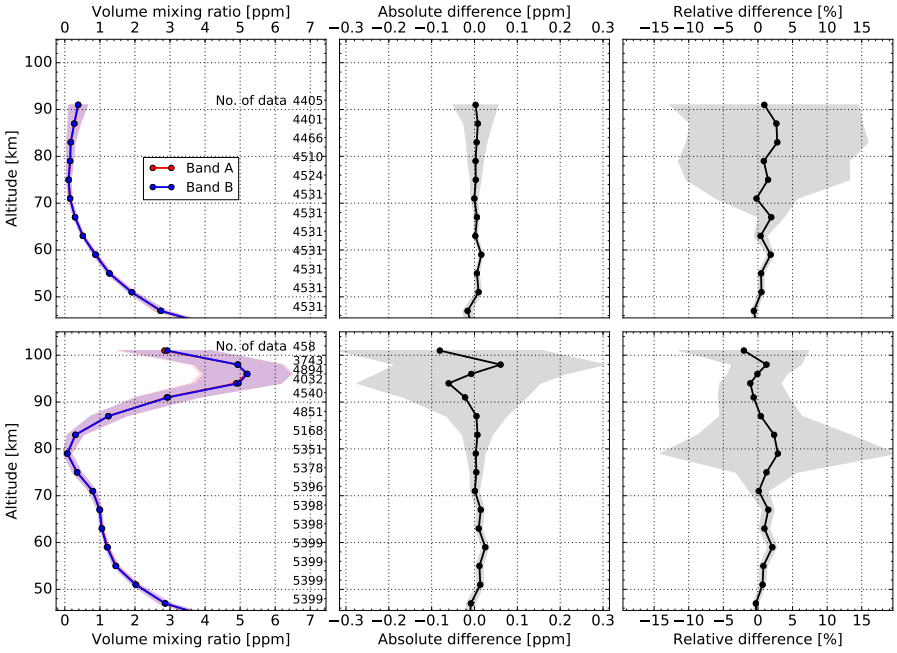

Figure 5: Comparison of the O_3 profiles retrieved from Band-A and Band-B when these frequency bands were operated simultaneously in the daytime (top) and nighttime (bottom). The left panels show the median VMR profiles for ozone from Band-A (red) and Band-B (blue). The value of the median absolute deviation is represented by the shaded area. The center and right panels are the absolute and relative differences, respectively, of the O_3 retrieved from Band-A and Band-B. The shaded area represents the value of the median absolute deviation of the absolute and relative differences.

quality selection criteria of the v2.4 are the status flag is equal to zero and the estimated precision is larger than zero [13].

Figure 6 shows the comparison of O_3 profiles between v215, v300, v2.4, and v310 using the median absolute difference. The data are from a latitudinal range of 30^o S and 30^o N in December 2009 for day and nighttime conditions. The v310 product with good quality criteria is plotted. The median and the median absolute difference of the absolute and relative differences are also plotted in Fig. 6. The v310 products with good quality criteria are also plotted in Fig. 6. The other products were interpolated to the altitude grid of v310 to calculate

the relative and absolute differences.

The v310 O_3 profiles in the MLT region show good agreement with those from v300 and v2.4 in the daytime and nighttime within the variability of the median absolute difference. There is a difference between v215 and the other datasets. The major reason is caused by the difference of the L1b spectrum version and the method of the determination of the tangent height, as described in Kasai et al [17]. The tangent height was retrieved from the O_3 spectra and was used to retrieve O_3 profiles in v215, which were very sensitive to the accuracy of non-linear gain calibration and introduced unwilling systematic errors. The tangent height information improved for L1b 008 using the neighboring Monitor of All-sky X-ray Image instrument from the SMILES instruments on the ISS.

The useful altitude ranges of the daytime ozone profiles were up to 92.0 and 97.5 km for the NICT-SMILES products and the JAXA-SMILES products, respectively. We found that the set-up of the a priori covariance matrix $\mathbf{S}_a$ used in the retrieval procedure caused differences in the upper limit of the O_3 amount. The value of a priori covariance was, e.g., 100 and 0.3 ppm^2 for JAXA-SMILES and NICT-SMILES, respectively, for the O_3 amount of 0.5 ppm at 95 km. The large variance of a priori covariance (20 times greater than the real profile) did not constrain a retrieval solution, particularly for the case spectrum SNR smaller than 1.0 around a tangent height above 90 km.

For the nighttime ozone profiles, useful altitude ranges were up to 92 km, 92 km, 101 km, and 100 km for v215, v300, v310, and v2.4, respectively. The reason for the difference between the NICT-SMILES products is caused by the difference in the window configurations as shown in Table 1. In the v310 O_3 profiles, the number of data at 101 km was less than at lower altitudes, and this corresponds to the maximum tangent height of the SMILES spectrum.

The random error was calculated from the sum of squares of the smoothing error and noise errors. The median percentage value of the random error for v310 nighttime ozone is about 5%, 50%, and 35% in the mesosphere, mesopause, and lower thermosphere, respectively. These values are almost the same with those in v215 and v300, but 30% smaller than that of v2.4. The random error

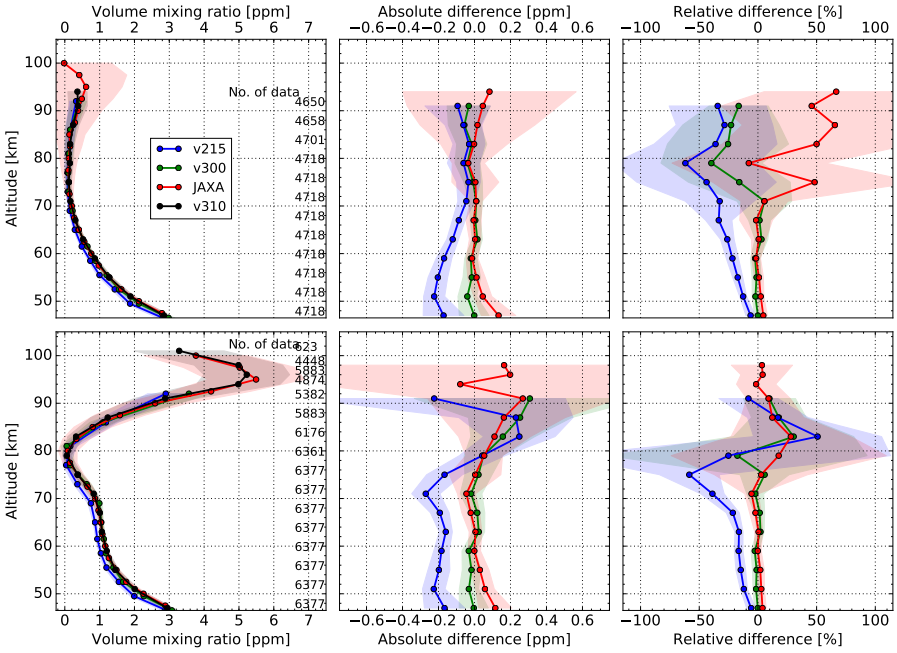

Figure 6: Comparison of the O_3 profiles retrieved from NICT-SMILES v310, v300, v215, and JAXA-SMILES v2.4 in the daytime (top) and nighttime (bottom). The left panels show the median VMR profiles for O_3 from NICT-SMILES v310 (black), v215 (blue), v300 (green), and JAXA-SMILES v2.4 (red). The shaded area represents the value of the median absolute deviation. The center and right panels are the absolute and relative differences, respectively, of O_3 between NICT-SMILES v310 and previous products. The shaded area represents the value of the median absolute deviation of the absolute and relative differences.

was reduced by the improvement of a priori information for the temperature, which maintained the continuous smooth change and internal consistency with altitude.

One of the improvements resulting from comparing the ozone profiles of the v310 products with previous SMILES products, is the nighttime O_3 profiles with the altitude step of 2 km around the secondary ozone maximum (95 km) with a random error of 35%. In addition, the quality criteria in the v310 processing forces omission of poor data, which were retrieved under low SNR conditions or low tangent heights of the SMILES spectrum.

4. Correlation of amount of O_3 and ClO at the polar region after sunset when ClO is enhanced

A scientific application of v310 O_3 profiles is shown in this section. In 2012, we noticed ClO enhancement around 70 km (ClO third peak) in a latitudinal range of 50^o N – 65^o N after sunset, in the polar region in the time range between January and February 2010 [30]. We found the correlation between $\boldsymbol{x}_{\mathrm{ClO}}$ (v215) and $\boldsymbol{x}_{\mathrm{O_3}}$ (v310) shows a positive trend, as shown in Fig. 7 (a), at 72.5 km in the latitudinal range of 50^o N – 65^o N in the SZA range of 90^o – 135^o in the time range between January and February 2010. The quality selection criteria included, where $\boldsymbol{m}$ is larger than 0.8 and smaller than 1.2, the χ^2 is smaller than 1.2, and the flag of the field of view conditions is smaller than 32 [12, 30]. The ClO (v215) was well validated already by Sato et al. [30] and Sagawa et al [31]. The systematic and random errors of v215 ClO products are about 10% and 100% around 70 km, respectively.

On the other hand, in the middle stratosphere, it is well-known that correlation between ClO (v215) and O_3 (v215) demonstrate a negative trend, as shown in Fig. 7 (b) at 32.5 km in the latitudinal range of 50^o N – 65^o N in the time range between January and February 2010, in the daytime. The negative correlation in the stratosphere is because of the well-known ClO catalytic cycle depleting O_3 by the reactions of $\mathrm{Cl} + \mathrm{O_3} \rightarrow \mathrm{ClO} + \mathrm{O_2}$ and $\mathrm{ClO} + \mathrm{O} \rightarrow \mathrm{Cl} + \mathrm{O_2}$.

In both atmospheric systems in the stratosphere and upper mesosphere, the amount of ClO is generally described as follows:

$$\frac{d[\mathrm{ClO}]}{dt} = k_1[\mathrm{Cl}][\mathrm{O_3}] + \mathrm{k_2}[\mathrm{ClO}][\mathrm{O}]. \tag{9}$$

Where the brackets represent the number density, and k_1 and k_2 are the reaction rates of $\mathrm{Cl} + \mathrm{O_3} \rightarrow \mathrm{ClO} + \mathrm{O_2}$ and $\mathrm{ClO} + \mathrm{O} \rightarrow \mathrm{Cl} + \mathrm{O_2}$, respectively.

We tried to understand the chemical mechanism of this enhancement of ClO with a positive trend of O_3 by an estimating of the correlation between O_3 (v310) and ClO (v215) from two-error regression treatments [32] using the following

regression line:

$$\boldsymbol{x}_{\mathrm{ClO}} = \alpha \times \boldsymbol{x}_{\mathrm{O_3}} + \beta, \tag{10}$$

where α is the slope and β is the intercept; $\boldsymbol{x}_{\mathrm{O_3}}$ is the v310 O_3 VMR, and $\boldsymbol{x}_{\mathrm{ClO}}$ is the v215 ClO VMR. The total errors were calculated to be the root sum of the squares of the retrieval errors and systematic errors for two-error regression treatments. The regression line calculated from estimated α and β is plotted in Fig. 7 (b) (thick red line); α and β were estimated to be $5.9 \times 10^{-5} \pm 0.4 \times 10^{-5} (1\sigma)$ and $12.0 \pm 3.6 (1\sigma)$ [ppt], respectively.

What is the meaning of α? Assuming $d[\mathrm{ClO}]/\mathrm{dt} = 0$ as steady state, then Eq. 9 can be written as

$$[\mathrm{ClO}] = \frac{k_1[\mathrm{Cl}]}{k_2[\mathrm{O}]}[\mathrm{O_3}]. \tag{11}$$

The α value will be equal to the value of $k_1[\mathrm{Cl}]/\mathrm{k_2[O]}$ in this assumption.

Here, we calculate $\alpha^{\mathrm{t}} = k_1[\mathrm{Cl}]/\mathrm{k_2[O]}$ value theoretically using the values taken from SD-WACCM model calculations for the SMILES observation condition at 72.5 km in the latitudinal range of 50^o N – 65^o N in the SZA range of 90^o – 135^o in the time range between January and February 2010. Following values were used to provide α^{t}: $k_1 = 9.2 \times 10^{-12}$ [$\mathrm{cm^3}$ $\mathrm{molecule^{-1}}$ $\mathrm{s^{-1}}$], $k_2 = 4.1 \times 10^{-11}$ [$\mathrm{cm^3}$ $\mathrm{molecule^{-1}}$ $\mathrm{s^{-1}}$], [Cl] = 9.4×10^4 [molecule $\mathrm{cm^{-3}}$], and [O] = 1.1×10^9 [molecule $\mathrm{cm^{-3}}$].

The theoretical α^{t} value becomes 1.9×10^{-5}, and agrees well with the one directly derived from the SMILES observation ($5.9 \times 10^{-5} \pm 0.4 \times 10^{-5} (1\sigma)$). This means that the simple chemical mechanism shown in Eq. 11 quantitatively described the enhancement of ClO VMR associated with the O_3 at 72.5 km in the latitudinal range of 50^o N – 65^o N in the SZA range of 90^o – 135^o in the time range between January and February 2010 well.

5. Conclusion

We have developed an optimal retrieval method for O_3 in the MLT region for submillimeter-wave limb emission spectra from space. We applied it to the

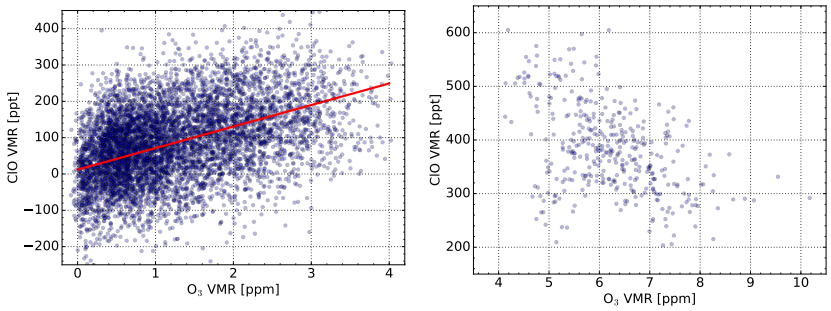

Figure 7: (a) The scatter plot displays the association between $\boldsymbol{x}_{\mathrm{ClO}}$ (v215) and $\boldsymbol{x}_{\mathrm{O_3}}$ (v310) at 72.5 km in the latitudinal range of 50^o N – 65^o N in the SZA range of 90^o – 135^o in the time range between January and February 2010. The regression line, plotted as a thick red line, was calculated from estimates of α and β. (b) The scatter plot displays the association between $\boldsymbol{x}_{\mathrm{ClO}}$ (v215) and $\boldsymbol{x}_{\mathrm{O_3}}$ (v215) at 32.5 km during the daytime in the latitudinal range of 50^o N – 65^o N in the time range between January and February 2010.

SMILES spectra and named SMILES v310 O_3 products. The optimal method included changes to the following retrieval configuration: 1) The retrieval vertical range is between 50 and 110 km, 2) The frequency window range is 120 MHz, 3) The vertical grids were 4-km and 2-km for 50–84 km and 84–101 km, respectively, and 4) Appropriate temporal-spatial maps of a priori profiles were provided, with O_3 coming from SD-WACCM model calculations, and pressure and temperature profiles provided from GAIA model calculations.

An evaluation of the ozone profiles for the v310 products was performed by error analysis, internal O_3 comparison, and comparisons with previous SMILES products. The relative difference between Band-A and Band-B is smaller than about 3% at all retrieved altitude grids. The estimated total systematic errors in the nighttime were about 6% in the MLT region excluding the mesopause. The total systematic error for the mesopause in the nighttime was about 10%. The random error was estimated at about 5%, 50%, and 35% in the mesosphere, mesopause, and lower thermosphere, respectively for nighttime ozone profiles in the MLT region. For daytime conditions, the total systematic errors were about 6% in the lower and middle mesospheres. The total systematic errors were about 8% and 12% in the upper mesosphere and lower thermosphere,

respectively. The random error was estimated about 5%, 50% below and above the middle mesosphere. We found that averaging the profiles does not provide a sufficient effect necessary to reduce the smoothing error in the case of small amounts of O_3, related to small SNR in the O_3 spectrum. A comparison of ozone profiles was conducted between the v310 and previous SMILES products. It was confirmed by comparisons and error analysis that the optimized retrieval method successfully produced SMILES O_3 (v310) in the MLT region.

For the v310 products, the useful altitude range was up to 92.0 km for the daytime ozone profiles, which was related to the SMILES spectrum with an SNR smaller than 1.0 around the tangent height above 90 km. That of the nighttime was 101.0 km with the altitude step of 2-km around secondary ozone maximum, with a random error of 35%. The v310 products achieved more fine-grid and lower random error compared with the previous SMILES products. In addition, the quality criteria in the v310 processing force the omission of the poor data, which were retrieved under low SNR conditions or low tangent heights of the SMILES spectrum.

A scientific application was also performed. We found a positive correlation between O_3 and ClO for the first time at nighttime in the upper mesosphere using the optimized O_3 vertical profile. The slope α was estimated to be $5.9 \times 10^{-5} \pm 0.4 \times 10^{-5} (1\sigma)$ from the positive correlation between O_3 and ClO at 72.5 km in the latitudinal range of 50^o N – 65^o N in the SZA range of 90^o – 135^o in the time range between January and February 2010.

Furthermore, we were successful in quantitatively explaining the chemical mechanism. We assumed α value is equal to the value of $k_1[\mathrm{Cl}]/\mathrm{k}_2[\mathrm{O}]$ in the pure reaction system $\mathrm{Cl} + \mathrm{O}_3 \rightarrow \mathrm{ClO} + \mathrm{O}_2$ and $\mathrm{ClO} + \mathrm{O} \rightarrow \mathrm{Cl} + \mathrm{O}_2$, the α^{t} value, calculated theoretically, was to be 1.9×10^{-5}, and agree well with the one directly derived from the SMILES observation. The simple chemical mechanism quantitatively well described the enhancement of ClO VMR associated with O_3.

Concerning future research, it will be important to reveal the diurnal and seasonal behaviors of ozone in the MLT region.

Acknowledgement

The JEM/SMILES mission is a joint project of the Japan Aerospace Exploration Agency (JAXA) and the National Institute of Information and Communications Technology (NICT). The authors wish to acknowledge H. Sagawa (Kyoto Sangyo University), K. Kikuchi (National Astronomical Observatory of Japan), S. Ochiai (NICT), M. Shiotani (Kyoto University), M. Suzuki (ISAS/JAXA) and colleagues at JAXA and NICT for managing and supporting the SMILES mission. The authors thank to H. Fujiwara (Seikei University) and T. O. Sato (NICT) for scientific discussion. The authors are also grateful to V. Limpasuvan (Coastal Carolina University) for providing the data of SD-WACCM calculations. This work was supported by a grant-in-Aid for JSPS Research Fellow (JP14J11927).

References

[1] R. E. Dickinson, Method of parameterization for infrared cooling between altitudes of 30 and 70 kilometers, Journal of Geophysical Research 78 (21) (1973) 4451–4457. doi:10.1029/JC078i021p04451.
URL http://dx.doi.org/10.1029/JC078i021p04451

[2] M. Jucker, S. Fueglistaler, G. K. Vallis, Stratospheric sudden warmings in an idealized GCM, Journal of Geophysical Research: Atmospheres 119 (19) (2014) 11,054–11,064. doi:10.1002/2014JD022170.
URL http://dx.doi.org/10.1002/2014JD022170

[3] W. F. J. Evans, E. J. Llewellyn, Measurements of mesospheric ozone from observations of the 1.27.μ band, Radio Science 7 (1) (1972) 45–50. doi:10.1029/RS007i001p00045.
URL http://dx.doi.org/10.1029/RS007i001p00045

[4] R. M. Bevilacqua, D. F. Strobel, M. E. Summers, J. J. Olivero, M. Allen, The seasonal variation of water vapor and ozone in the upper mesosphere:

Implications for vertical transport and ozone photochemistry, Journal of Geophysical Research: Atmospheres 95 (D1) (1990) 883–893. doi:10.1029/JD095iD01p00883.
URL http://dx.doi.org/10.1029/JD095iD01p00883

[5] M. Kaufmann, O. A. Gusev, K. U. Grossmann, F. J. Martn-Torres, D. R. Marsh, A. A. Kutepov, Satellite observations of daytime and nighttime ozone in the mesosphere and lower thermosphere, Journal of Geophysical Research: Atmospheres 108 (D9) (2003) n/a–n/a, 4272. doi:10.1029/2002JD002800.
URL http://dx.doi.org/10.1029/2002JD002800

[6] A. K. Smith, M. López-Puertas, B. Funke, M. García-Comas, M. G. Mlynczak, L. A. Holt, Nighttime ozone variability in the high latitude winter mesosphere, J. Geophys. Res. Atmos. (119) (2014) 13,547 – 13,564. doi:10.1002/2014JD021987.

[7] R. R. Garcia, S. Solomon, A numerical model of the zonally averaged dynamical and chemical structure of the middle atmosphere, Journal of Geophysical Research: Oceans 88 (C2) (1983) 1379–1400. doi:10.1029/JC088iC02p01379.
URL http://dx.doi.org/10.1029/JC088iC02p01379

[8] A. K. Smith, D. R. Marsh, Processes that account for the ozone maximum at the mesopause, Journal of Geophysical Research: Atmospheres 110 (D23) (2005) n/a–n/a, d23305. doi:10.1029/2005JD006298.
URL http://dx.doi.org/10.1029/2005JD006298

[9] N. J. Livesey, W. G. Read, P. A. Wagner, L. Froidevaux, A. Lambert, G. L. Manney, L. F. Millán Valle, H. C. Pumphrey, M. L. Santee, M. J. Schwartz, S. Wang, R. A. Fuller, R. F. Jarnot, B. W. Knosp, E. Martinez, Version 4.2x Level 2 data quality and description document, Jet Propulsion Laboratory, tech. Rep. JPL D-33509 Rev. B (2016).

URL http://mls.jpl.nasa.gov/data/v4-2_data_quality_document.pdf

[10] U. Frisk, M. Hagström, J. AlaLaurinaho, S. Andersson, J. C. Berges, J. P. Chabaud, M. Dahlgren, A. Emrich, H. G. Florén, G. Florin, M. Fredrixon, T. Gaier, R. Haas, T. Hirvonen, A. Hjalmarsson, B. Jakobsson, P. Jukkala, P. S. Kildal, E. Kollberg, J. Lassing, A. Lecacheux, P. Lehikoinen, A. Lehto, J. Mallat, C. Marty, D. Michet, J. Narbonne, M. Nexon, M. Olberg, A. O. H. Olofsson, G. Olofsson, A. Origné, M. Petersson, P. Piironen, R. Pons, D. Pouliquen, I. Ristorcelli, C. Rosolen, G. Rouaix, A. V. Räisänen, G. Serra, F. Sjöberg, L. Stenmark, S. Torchinsky, J. Tuovinen, C. Ullberg, E. Vinterhav, N. Wadefalk, H. Zirath, P. Zimmermann, R. Zimmermann, The odin satellite, A&A 402 (3) (2003) L27–L34. doi:10.1051/0004-6361:20030335.

[11] J. W. Waters, L. Froidevaux, R. S. Harwood, R. F. Jarnot, H. M. Pickett, W. G. Read, P. H. Siegel, R. E. Cofield, M. J. Filipiak, D. A. Flower, J. R. Holden, G. K. Lau, N. J. Livesey, G. L. Manney, H. C. Pumphrey, M. L. Santee, D. L. Wu, D. T. Cuddy, R. R. Lay, M. S. Loo, V. S. Perun, M. J. Schwartz, P. C. Stek, R. P. Thurstans, M. A. Boyles, K. M. Chandra, M. C. Chavez, G.-S. Chen, B. V. Chudasama, R. Dodge, R. A. Fuller, M. A. Girard, J. H. Jiang, Y. Jiang, B. W. Knosp, R. C. LaBelle, J. C. Lam, K. A. Lee, D. Miller, J. E. Oswald, N. C. Patel, D. M. Pukala, O. Quintero, D. M. Scaff, W. V. Snyder, M. C. Tope, P. A. Wagner, M. J. Walch, The Earth observing system microwave limb sounder (EOS MLS) on the aura Satellite, IEEE Transactions on Geoscience and Remote Sensing 44 (5) (2006) 1075–1092. doi:10.1109/TGRS.2006.873771.

[12] D. Kreyling, H. Sagawa, I. Wohltmann, R. Lehmann, Y. Kasai, SMILES zonal and diurnal variation climatology of stratospheric andmesospheric trace gasses: O3, HCl, HNO3, ClO, BrO, HOCl,HO2, and temperature, Journal of Geophysical Research: Atmospheres 118 (20) (2013) 11,888–

11,903. doi:10.1002/2012JD019420.
URL http://dx.doi.org/10.1002/2012JD019420

[13] K. Imai, N. Manago, C. Mitsuda, Y. Naito, E. Nishimoto, T. Sakazaki, M. Fujiwara, L. Froidevaux, T. von Clarmann, G. P. Stiller, D. P. Murtagh, P.-p. Rong, M. G. Mlynczak, K. A. Walker, D. E. Kinnison, H. Akiyoshi, T. Nakamura, T. Miyasaka, T. Nishibori, S. Mizobuchi, K.-i. Kikuchi, H. Ozeki, C. Takahashi, H. Hayashi, T. Sano, M. Suzuki, M. Takayanagi, M. Shiotani, Validation of ozone data from the Superconducting Submillimeter-Wave Limb-Emission Sounder (SMILES), Journal of Geophysical Research: Atmospheres 118 (11) (2013) 5750–5769. doi:10.1002/jgrd.50434.

[14] T. Sakazaki, M. Fujiwara, C. Mitsuda, K. Imai, N. Manago, Y. Naito, T. Nakamura, H. Akiyoshi, D. Kinnison, T. Sano, M. Suzuki, M. Shiotani, Diurnal ozone variations in the stratosphere revealed in observations from the superconducting submillimeter-wave limb-emission sounder (SMILES) on board the international space station (ISS), Journal of Geophysical Research: Atmospheres 118 (7) (2013) 2991–3006. doi:10.1002/jgrd.50220.
URL http://dx.doi.org/10.1002/jgrd.50220

[15] A. K. Smith, V. L. Harvey, M. G. Mlynczak, B. Funke, M. García-Comas, M. Hervig, M. Kaufmann, E. Kyrölä, M. López-Puertas, I. McDade, C. E. Randall, J. M. Russell, P. E. Sheese, M. Shiotani, W. R. Skinner, M. Suzuki, K. A. Walker, Satellite observations of ozone in the upper mesosphere, Journal of Geophysical Research: Atmospheres 118 (11) (2013) 5803–5821. doi:10.1002/jgrd.50445.

[16] K. Sagi, D. Murtagh, J. Urban, H. Sagawa, Y. Kasai, The use of SMILES data to study ozone loss in the arctic winter 2009/2010 and comparison with Odin/SMR data using assimilation techniques, Atmospheric Chemistry and Physics 14 (23) (2014) 12855–12869. doi:10.5194/acp-14-12855-2014.
URL http://www.atmos-chem-phys.net/14/12855/2014/

[17] Y. Kasai, H. Sagawa, D. Kreyling, K. Suzuki, E. Dupuy, T. O. Sato, J. Mendrok, P. Baron, T. Nishibori, S. Mizobuchi, K. Kikuchi, T. Manabe, H. Ozeki, T. Sugita, M. Fujiwara, Y. Irimajiri, K. A. Walker, P. F. Bernath, C. Boone, G. Stiller, T. von Clarmann, J. Orphal, J. Urban, D. Murtagh, E. J. Llewellyn, D. Degenstein, A. E. Bourassa, N. D. Lloyd, L. Froidevaux, M. Birk, G. Wagner, F. Schreier, J. Xu, P. Vogt, T. Trautmann, M. Yasui, Validation of stratospheric and mesospheric ozone observed by SMILES from International Space Station, Atmos. Meas. Tech. (6) (2013) 2311–2338. doi:10.5194/amt-6-2311-2013.

[18] H. M. Pickett, R. L. Poynter, E. A. Cohen, M. L. Delitsky, J. C. Pearson, H. S. P. Müller, Submillimeter, Millimeter, and Microwave Spectral Line Catalog, Journal of Quantitative Spectroscopy and Radiative Transfer 60 (5) (1998) 883–890. doi:10.1016/S0022-4073(98)00091-0.

[19] P. Baron, J. Urban, H. Sagawa, J. Möller, D. P. Murtagh, J. Mendrok, E. Dupuy, T. O. Sato, S. Ochiai, K. Suzuki, T. Manabe, T. Nishibori, K. Kikuchi, R. Sato, M. Takayanagi, Y. Murayama, M. Shiotani, Y. Kasai, The Level 2 research product algorithms for the Superconducting Submillimeter-Wave Limb-Emission Sounder (SMILES), Atmospheric Measurement Techniques 4 (10) (2011) 2105–2124. doi:10.5194/amt-4-2105-2011.

[20] C. Takahashi, S. Ochiai, M. Suzuki, Operational retrieval algorithms for JEM/SMILES level 2 data processing system, Journal of Quantitative Spectroscopy and Radiative Transfer 111 (1) (2010) 160–173. doi:10.1016/j.jqsrt.2009.06.005.

[21] S. Ochiai, K. Kikuchi, T. Nishibori, S. Mizobuchi, T. Manabe, Calibration of superconducting submillimeter-wave limb-emission sounder (SMILES) on the ISS, Proc. SPIEdoi:10.1117/12.977370.

[22] M. Rienecker, M. Suarez, R. Todling, J. Bacmeister, L. Takacs, H.-C. Liu, W. Gu, M. Sienkiewicz, R. Koster, R. Gelaro, I. Stajner, J. Nielsen, The

GEOS-5 Data Assimilation System – Documentation of Versions 5.0.1, 5.1.0, and 5.2.0, Tech. Rep. NASA/TM2008104606, National Aeronautics and Space Administration, Goddared (2008).
URL https://gmao.gsfc.nasa.gov/pubs/docs/Rienecker369.pdf

[23] L. Froidevaux, N. J. Livesey, W. G. Read, Y. B. Jiang, C. Jimenez, M. J. Filipiak, M. J. Schwartz, M. L. Santee, H. C. Pumphrey, J. H. Jiang, D. L. Wu, G. L. Manney, B. J. Drouin, J. W. Waters, E. J. Fetzer, P. F. Bernath, C. D. Boone, K. A. Walker, K. W. Jucks, G. C. Toon, J. J. Margitan, B. Sen, C. R. Webster, L. E. Christensen, J. W. Elkins, E. Atlas, R. A. Lueb, R. Hendershot, Early validation analyses of atmospheric profiles from EOS MLS on the aura Satellite, IEEE Transactions on Geoscience and Remote Sensing 44 (5) (2006) 1106–1121. doi:10.1109/TGRS.2006.864366.

[24] J.-F. Lamarque, L. K. Emmons, P. G. Hess, D. E. Kinnison, S. Tilmes, F. Vitt, C. L. Heald, E. A. Holland, P. H. Lauritzen, J. Neu, J. J. Orlando, P. J. Rasch, G. K. Tyndall, CAM-chem: description and evaluation of interactive atmospheric chemistry in the Community Earth System Model, Geoscientific Model Development 5 (2) (2012) 369–411. doi:10.5194/gmd-5-369-2012.
URL http://www.geosci-model-dev.net/5/369/2012/

[25] O. V. Tweedy, V. Limpasuvan, Y. J. Orsolini, A. K. Smith, R. R. Garcia, D. Kinnison, C. E. Randall, O.-K. Kvissel, F. Stordal, V. L. Harvey, A. Chandran, Nighttime secondary ozone layer during major stratospheric sudden warmings in specified-dynamics WACCM, Journal of Geophysical Research: Atmospheres 118 (15) (2013) 8346–8358. doi:10.1002/jgrd.50651.
URL http://dx.doi.org/10.1002/jgrd.50651

[26] M. M. Rienecker, M. J. Suarez, R. Gelaro, R. Todling, J. Bacmeister, E. Liu, M. G. Bosilovich, S. D. Schubert, L. Takacs, G.-K. Kim, S. Bloom, J. Chen, D. Collins, A. Conaty, A. da Silva, W. Gu, J. Joiner, R. D. Koster, R. Luc-

chesi, A. Molod, T. Owens, S. Pawson, P. Pegion, C. R. Redder, R. Reichle, F. R. Robertson, A. G. Ruddick, M. Sienkiewicz, J. Woollen, MERRA: NASAs Modern-Era Retrospective Analysis for Research and Applications, Journal of Climate 24 (14) (2011) 3624–3648. arXiv:http://dx.doi.org/10.1175/JCLI-D-11-00015.1, doi:10.1175/JCLI-D-11-00015.1.
URL http://dx.doi.org/10.1175/JCLI-D-11-00015.1

[27] A. E. Hedin, Extension of the MSIS Thermosphere Model into the middle and lower atmosphere, Journal of Geophysical Research: Space Physics 96 (A2) (1991) 1159–1172. doi:10.1029/90JA02125.

[28] H. Jin, Y. Miyoshi, D. Pancheva, P. Mukhtarov, H. Fujiwara, H. Shinagawa, Response of migrating tides to the stratospheric sudden warming in 2009 and their effects on the ionosphere studied by a whole atmosphere-ionosphere model GAIA with COSMIC and TIMED/SABER observations, Journal of Geophysical Research: Space Physics 117 (A10) (2012) n/a–n/a, a10323. doi:10.1029/2012JA017650.
URL http://dx.doi.org/10.1029/2012JA017650

[29] Y. J. Kasai, J. Urban, C. Takahashi, S. Hoshino, K. Takahashi, J. Inatani, M. Shiotani, H. Masuko, Stratospheric ozone isotope enrichment studied by submillimeter wave heterodyne radiometry: the observation capabilities of smiles, IEEE Transactions on Geoscience and Remote Sensing 44 (3) (2006) 676–693. doi:10.1109/TGRS.2005.861754.

[30] T. O. Sato, H. Sagawa, D. Kreyling, T. Manabe, S. Ochiai, K. Kikuchi, P. Baron, J. Mendrok, J. Urban, D. Murtagh, M. Yasui, Y. Kasai, Strato-mesospheric ClO observations by SMILES: error analysis and diurnal variation, Atmos. Meas. Tech. (5) (2012) 2809–2825. doi:10.5194/amt-5-2809-2012.

[31] H. Sagawa, T. O. Sato, P. Baron, E. Dupuy, N. Livesey, J. Urban, T. von Clarmann, A. de Lange, G. Wetzel, A. Kagawa, D. Murtagh, Y. Kasai, Comparison of SMILES ClO profiles with other satellite and balloon-based

measurements, Atmos. Meas. Tech. Discuss. (6) (2013) 613–663. doi:10.5194/amtd-6-613-2013.

[32] C. Brooks, S. R. Hart, I. Wendt, Realistic use of two-error regression treatments as applied to rubidium-strontium data, Reviews of Geophysics 10 (2) (1972) 551–577. doi:10.1029/RG010i002p00551.
URL http://dx.doi.org/10.1029/RG010i002p00551